ELSEVIER

Ceramics International 31 (2005) 795–802

CERAMICS INTERNATIONAL

www.elsevier.com/locate/ceramint

Synthesis of nanocrystalline cerium oxide particles by the precipitation method

Huey-Ing Chen*, Hung-Yi Chang

Department of Chemical Engineering, National Cheng Kung University, Tainan 70101, Taiwan, ROC

Received 12 March 2004; received in revised form 25 August 2004; accepted 15 September 2004
Available online 9 December 2004

Abstract

Effects of reaction temperature and atmosphere on properties of the CeO_2 particles prepared by the precipitation technique, including particle size, shape, and crystalline structure were investigated. Also, the bandgap energies were estimated from the UV absorption spectra. Experimental results showed that the prepared particles were primary, non-porous and with cubic fluorite structure. The reaction temperature and oxygen content of O_2/N_2 atmosphere played important roles on the size and shape of resulting particles. The average particle size as well as the crystallite size increased with increasing the reaction temperature and decreasing the oxygen content. Besides, the particle shape transformed from square-like to hexagonal as the temperature was raised from 30 to 90 °C. In oxygen-lean atmosphere, the shape of all resulting particles was hexagonal, whereas needles mixed with hexagonal particles found at above 50% O_2. Due to the quantum confinement effect, the bandgap energies of particles over the studied conditions approximately increased with decreasing particle size. However, the oxygen-induced shape change exhibited an exceptional deviation.

Keywords: A. Powders: chemical preparation; C. Optical properties; D. CeO_2; Nanoparticles

1. Introduction

In recent years, nanocrystalline cerium oxide (CeO_2) particles have been extensively studied owing to their potential uses in many applications, such as UV absorbents and filters [1,2], buffer layers with silicon wafer [3], gas sensors [4], catalysts in the fuel cell technology [5–7], catalytic wet oxidation [8], engine exhaust catalysts [9], NO removal [10], photocatalytic oxidation of water [11], etc. However, the material performances in practical uses are strongly influenced by the properties of constituent CeO_2 particles.

Numerous techniques have been proposed to synthesize nano-sized CeO_2 particles with promising control of properties, such as hydrothermal [12–16], reverse micelles [1,17], sonochemical [18], pyrolysis [19] and homogeneous precipitation [2,20–24]. Among them, owing to the advantages of simple process, easy scale-up and low cost, the precipitation technique has attracted the most extensive attentions. For example, Zhou et al. [20] produced CeO_2 particles of about 4 nm from cerium nitrate and ammonia. Matijević and Hsu [21] prepared sub-micron $Ce_2O(CO_3)_2{\cdot}H_2O$ particles from cerium nitrate with urea. Chen and Chen [22] prepared CeO_2 particles from cerium nitrate with hexamethylenetetramine, whereas Li et al. [23] used ammonia carbonate and diethylamine as the precipitate agents. Yamashita et al. [2] produced CeO_2 particles from cerium chloride and sodium hydroxide with the presence of hydrogen peroxide under various pH conditions from 6 to 12. Uekawa et al. [24] obtained 7–9 nm CeO_2 particles starting from cerium nitrate in the polyethylene glycol solution. Although CeO_2 particles prepared by the precipitation technique have been extensively studied, most of the previous reports were focused on effects of cerium precursors, ligands, additives and reaction media. Less information was reported on the influences of reaction temperature and atmosphere. Therefore, in the present work,

* Corresponding author. Tel.: +886 6 2757575; fax: +886 6 2344496.
E-mail address: hueying@mail.ncku.edu.tw (H.-I. Chen).

0272-8842/$30.00
doi:10.1016/j.ceramint.2004.09.006

it was attempted to study the effects of reaction temperature and oxygen content of atmosphere on the formation of CeO_2 particles. The particle size, morphology, shape, crystalline structure and UV absorption of resulting particles were also demonstrated and discussed.

2. Experimental

All chemicals were reagent grade and used without further purification. A 50 ml of aqueous cerium nitrate ($Ce(NO_3)_3{\cdot}6H_2O$, Strem, 99.9%) solution (0.2 M) was used as the cerium precursor. Firstly, 25 ml of ammonia water (from Riedel-de Haën Co.) was totally added into the cerium precursor solution. The reaction was carried out at the desired temperature with a stirring rate of 500 rpm. A stream of O_2/N_2 mixture was bubbled into the reactor to oxidize Ce(III) to Ce(IV). The oxygen content of the atmosphere for this study was ranged from 5% to pure oxygen, which was measured with a gas chromatograph (GC14B, Shimadzu). At the beginning of reaction, a white precipitate came out in the solution immediately. Subsequently, the color of precipitates turned into purple, and gradually became light yellow. The time required for completing the reaction was 2 h. Finally, the precipitate was centrifuged, and followed by washing with de-ionized water and ethanol alternatively for three times.

The pH value of the reaction solution was recorded with a pH meter (HM-20S, TOA, Japan). The morphologies of as-prepared CeO_2 nanoparticles were observed by TEM (1200EX, JEOL). An appropriate amount of CeO_2 suspension was dropped onto carbon-coated copper grids for TEM observation. The average particle size (d_{TEM}) and particle size distribution were determined from TEM images by counting more than 100 particles. However, needle-like particles were excluded from the size calculation. The HRTEM (3010, JEOL) with an accelerating voltage of 300 kV was employed for larger magnified observations. The crystalline structure was studied by using XRD (RX-III, Rigaku), and the crystallite size of samples, d_{XRD}, was estimated by applying full-width-half-maximum (FWHM) of characteristic peak (1 1 1) to the Scherrer equation:

$$d_{XRD} = \frac{0.9\lambda}{\mathrm{FWHM}\cos\theta} \quad (1)$$

where λ was the incident wavelength (1.5406 Å in this study) of X-ray, and θ was the diffraction angle for the (1 1 1) plane. The particle size of samples measured by nitrogen adsorption at 77 K (ASAP 2010, Micromeritics), d_{BET}, was calculated by using the Brunauer–Emmett–Teller (BET) equation with assuming that the CeO_2 particles were spherical and non-porous [20]. The bandgap energies of samples were estimated from the UV–vis absorption spectra (UV–vis spectrophotometer, Lambda 20, Perkin Elmer). The sample loading in ethanol for the measurement was in range of 0.08–0.15 g/L.

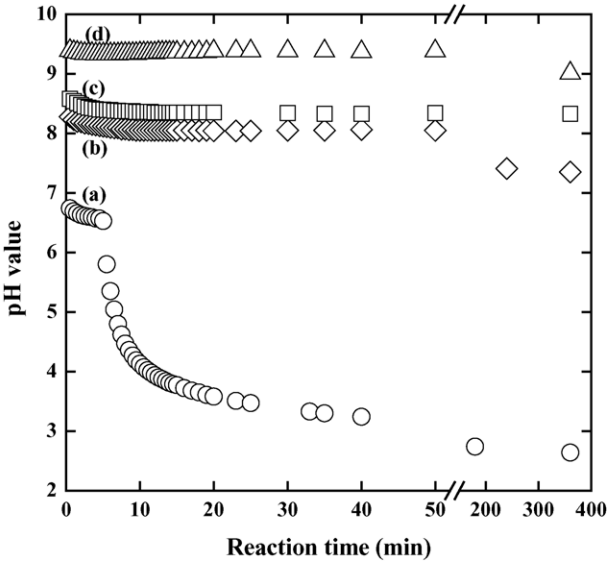

Fig. 1. The pH evolution for $[NH_4OH]$: (a) 1.2 M, (b) 2.0 M, (c) 3.0 M, and (d) 6.0 M. $[Ce^{3+}]_0$ = 0.2 M, reaction temperature = 70 °C.

3. Results and discussion

3.1. CeO_2 formation mechanism and pH evolution

The formation of CeO_2 involves several complicated reactions [25–27]. As the ammonia water is totally added into the cerium precursor solution, the $Ce(OH)_3$ precipitate is formed immediately due to the extreme low solubility constant (7×10^{-21}) [26]. Subsequently, the $Ce(OH)_3$ was oxidized to hydrated Ce(IV) ions in alkaline environment [27], and then further hydrolyzed to form $[Ce(OH)_x(H_2O)_y]^{(4-x)+}$ complex [13,22]. Finally, the cer-

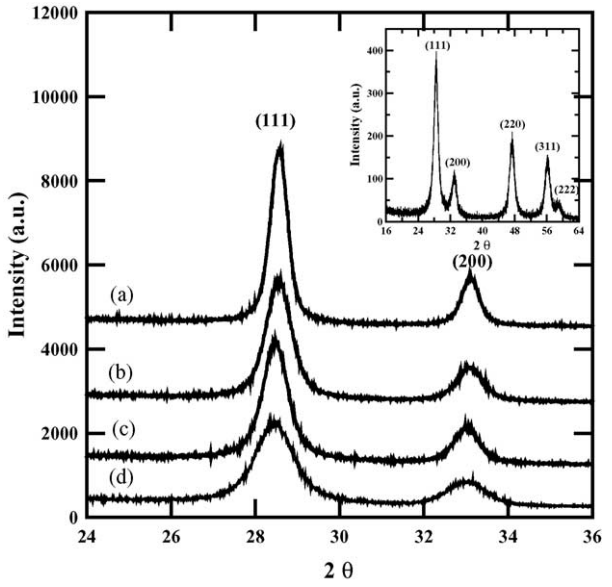

Fig. 2. XRD patterns for CeO_2 particles prepared at different temperatures: (a) 30 °C, (b) 50 °C, (c) 70 °C, and (d) 90 °C. $[Ce^{3+}]_0$ = 0.2 M, $[NH_4OH]$ = 3.0 M.

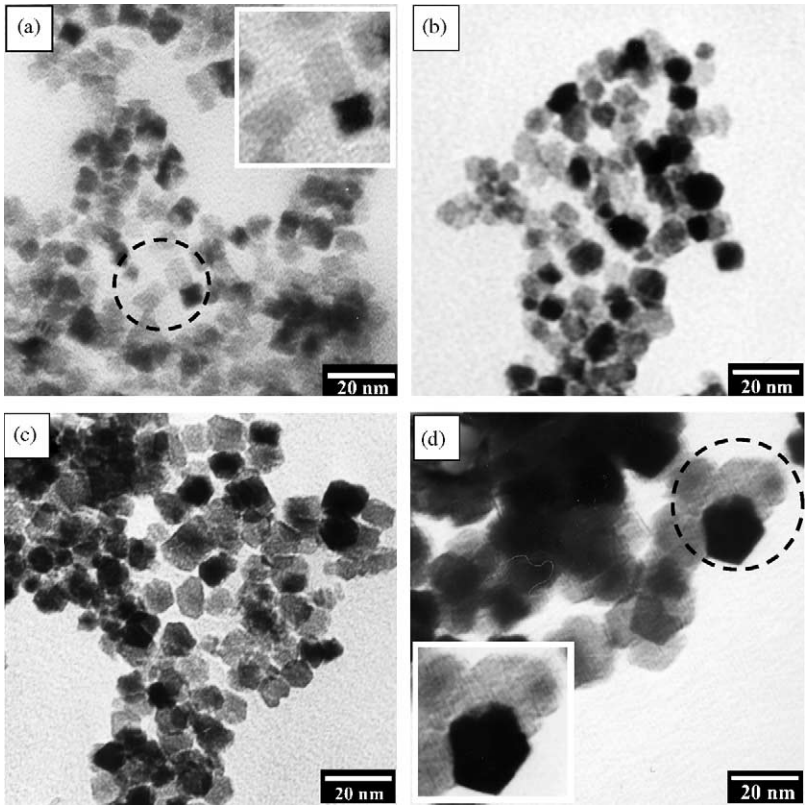

Fig. 3. TEM images of CeO_2 particles prepared at different temperatures: (a) 30 °C, (b) 50 °C, (c) 70 °C, and (d) 90 °C. $[Ce^{3+}]_0$ = 0.2 M, $[NH_4OH]$ = 3.0 M.

ium(IV) hydroxide complex is deprotonated by water molecules to form cerium oxide (CeO_2) [27]. It is noticed that the hydroxyl ions are highly involved in the whole process, which would strongly affect the supersaturation degree of initial precipitate [20] and the oxidation of Ce(III) to Ce(IV) [22]. Therefore, the concentration of hydroxyl ions, i.e., alternatively indicated by the pH of solution, plays an important role on determining the particle morphology [2] and the resulting suspension state [27]. Since the evolution of pH value indeed corresponds to the extent of reaction, monitoring the pH change is helpful to comprehend the formation mechanism of CeO_2 particles.

The variation of pH with reaction time at different ammonia concentrations is shown in Fig. 1. As the concentration of ammonia water is 1.2 M, the pH value decreases slowly within initial 5 min and then falls down abruptly. The abrupt pH drop indicates that considerable hydroxyl ions are consumed in this stage. Zhou et al. [20] and Chen and Chen [22] reported, higher concentration of hydroxyl ions would favor the Ce(III)/Ce(IV) oxidation, and moreover, the hydronium ions (H_3O^+) were released accompanying with the Ce(III)/Ce(IV) oxidation and causing the sharp decrease of pH. In the subsequent hydrolysis and deprotonation steps, hydroxyl ions are substantially depleted at a slower rate. Even though the reaction time is further prolonged to 400 min, the pH value decreases no more, which reveals the dissolution and recrystallization of particles are performed in this stage. At

Table 1
Average particle size and crystallite size of CeO_2 nanoparticles obtained at various preparation conditions

Reaction condition	$[Ce^{3+}]_0$ (M)	$[NH_4OH]$ (M)	Atmosphere	d_{TEM} (nm)	d_{XRD} (nm)	d_{BET} (nm)
90 °C, 2 h	0.2	3.0	Air	18.8 ± 2.9	16.4	15.8
70 °C, 2 h	0.2	3.0	Air	12.0 ± 1.5	11.5	12.1
50 °C, 2 h	0.2	3.0	Air	10.6 ± 1.4	10.9	10.8
30 °C, 2 h	0.2	3.0	Air	7.4 ± 1.1	7.4	7.1
70 °C, 2 h	0.2	3.0	5% O_2[a]	15.9 ± 2.5	13.4	–
70 °C, 2 h	0.2	3.0	21% O_2[a]	12.0 ± 1.5	11.5	12.1
70 °C, 2 h	0.2	3.0	50% O_2[a]	11.1 ± 1.5[b]	9.1	–
70 °C, 2 h	0.2	3.0	73% O_2[a]	9.2 ± 1.5[b]	8.6	–
70 °C, 2 h	0.2	3.0	Pure O_2	9.4 ± 2.3[b]	7.9	–

[a] Oxygen percentage in O_2/N_2 mixture.
[b] Needle-like particles are excluded from the size calculation.

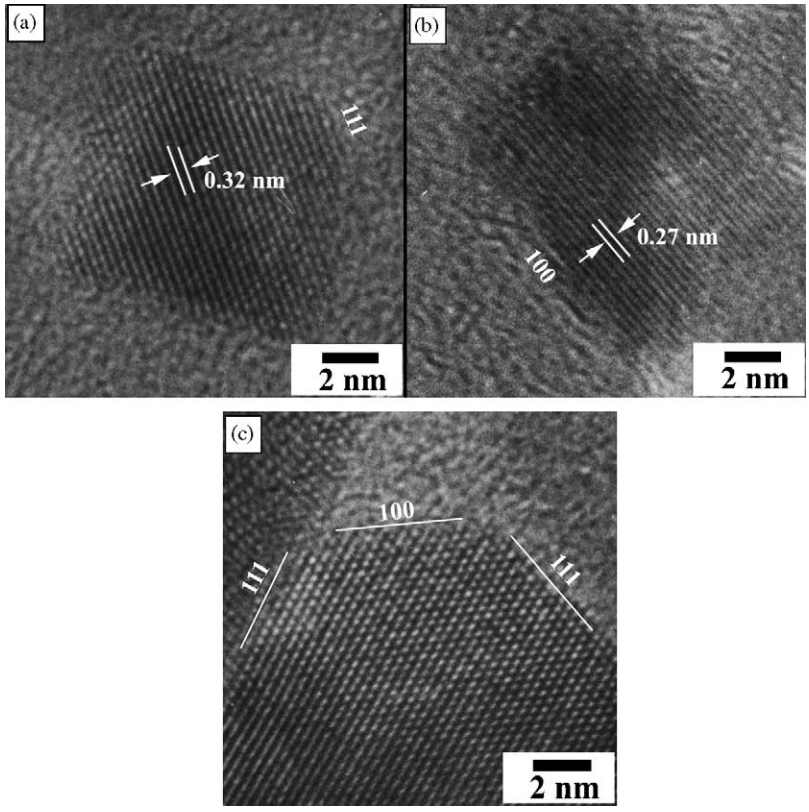

Fig. 4. HRTEM images for CeO_2 particles prepared at (a) 30 °C: {1 1 1} facets, (b) 30 °C: {1 0 0} facets, and (c) 90 °C.

ammonia concentration of 3 M, since the hydroxyl ions are in large excess, the pH value can nearly remain constant during the whole process. Consequently, in order for achieving uniform particles, 3 M of ammonia water is employed to ensure the reaction occurred at pH 9.5.

3.2. Effect of reaction temperature

The typical XRD pattern of prepared CeO_2 particles is shown as the inset of Fig. 2. The characteristic peaks are very close to the cubic fluorite structured CeO_2 crystal in the JCPDS database. Besides, the XRD patterns in 2θ ranges of 25–35° (Fig. 2) show that samples prepared at lower temperatures exhibit broader peaks shifting toward a little smaller angles.

The TEM images of CeO_2 nanoparticles prepared at 30, 50, 70, and 90 °C (Fig. 3) demonstrate fairly uniform size distributions. Moreover, the particle size increases with elevating the reaction temperature, inferred that the growth rate of particles is predominant over the nucleation rate. This result is in good agreement with that reported by Wu et al. [12]. As shown in Table 1, the average particle size obtained from TEM (d_{TEM}) is quite close to the crystallite size obtained from XRD patterns (d_{XRD}). This clearly indicates the presence of agglomerates in CeO_2 particles can be neglected at various reaction temperatures. In addition, the BET average particle size, d_{BET}, based on assumptions of non-porous and spherical particles, shows very good consistence with d_{XRD} and d_{TEM}. Therefore, the prepared particles are confirmed to be primary and non-porous.

From Fig. 3, the shape of CeO_2 particles is strongly dependent on the reaction temperature. At 30 °C, the prepared particles are shaped square-like, whereas they are transformed into hexagonal shape at higher temperature. To

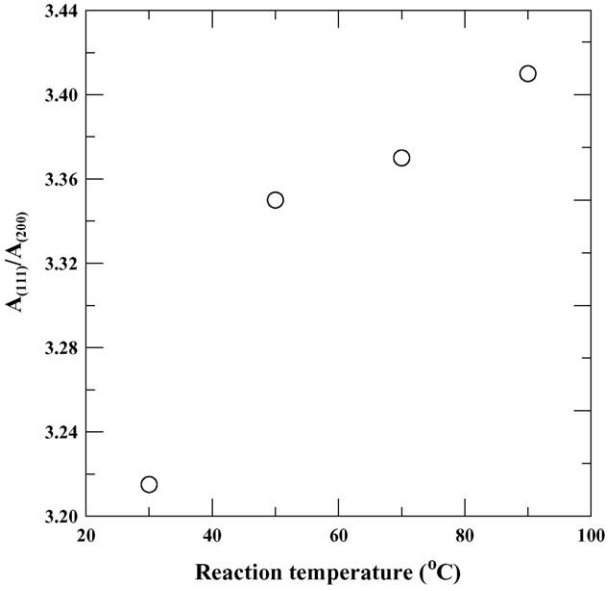

Fig. 5. Dependence of $A_{(1\ 1\ 1)}/A_{(2\ 0\ 0)}$ ratio on the reaction temperature.

further observe the particles obtained at 30 °C by HRTEM, two square-like crystals with truncated corners are shown in Fig. 4a and b, respectively. One is with {1 1 1} facets which grow along the diagonal direction (Fig. 4a), and the other is with {1 0 0} facets which are along the edge of square (Fig. 4b). The interplanar spacings for {1 1 1} and {1 0 0} facets are determined as 0.32 and 0.27 nm, respectively. As raising the reaction temperature to 90 °C, larger particles are appeared (Fig. 4c). Besides, since the {1 0 0} facets with higher surface energy grow slower than {1 1 1} facets, it results in the particles growing from truncated cubes to cubo-octahedrons, and thus the corresponding images transforming from square-like to hexagonal shape [28,29]. Alternatively, the shape evolution can also be confirmed by the XRD patterns. The intensity ratio of plane (1 1 1) to (2 0 0), $A_{(1\ 1\ 1)}/A_{(2\ 0\ 0)}$, increases with increasing the reaction temperature (Fig. 5). Obviously, this depicts the occurrence probability of plane (1 1 1) is predominant over the plane (2 0 0), which is in good accordance with the HRTEM results and also agrees with reports of Kirk and Wood [30].

3.3. Effect of atmosphere

In the presence of oxygen, the precipitates of $Ce(OH)_3$ is transformed to CeO_2 according to the following equation:

$$2Ce(OH)_3 + \frac{1}{2}O_2 \rightarrow 2CeO_2 + 3H_2O \quad (2)$$

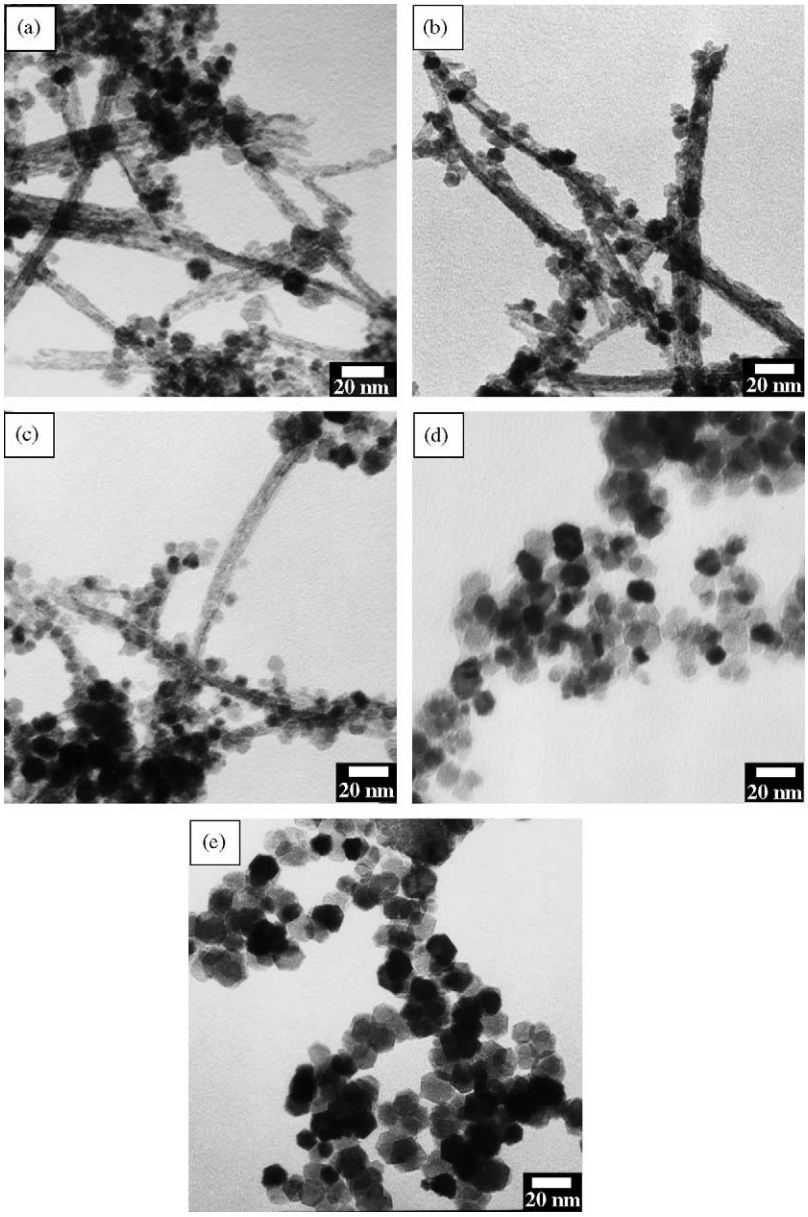

Fig. 6. TEM images of CeO_2 particles prepared under oxygen content of O_2–N_2 atmosphere: (a) 100%, (b) 73%, (c) 50%, (d) 21%, and (e) 5%. $[Ce^{3+}]_0$ = 0.2 M, $[NH_4OH]$ = 3.0 M, temperature = 70 °C.

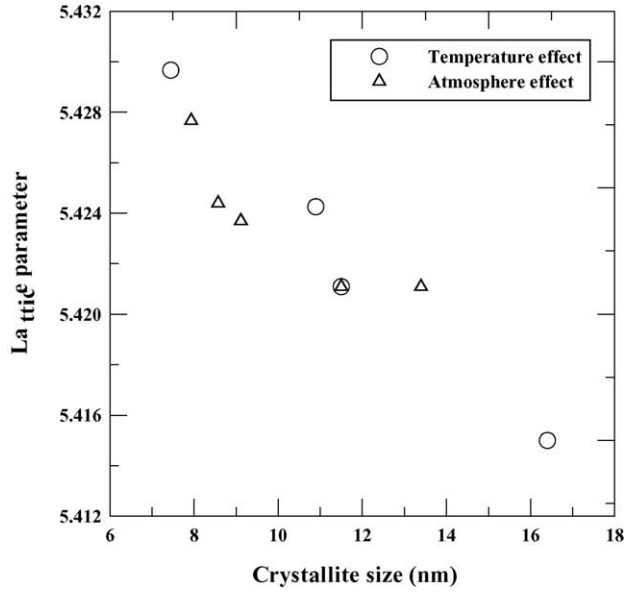

Fig. 7. The relationship between lattice parameter and crystallite size of CeO_2 particles.

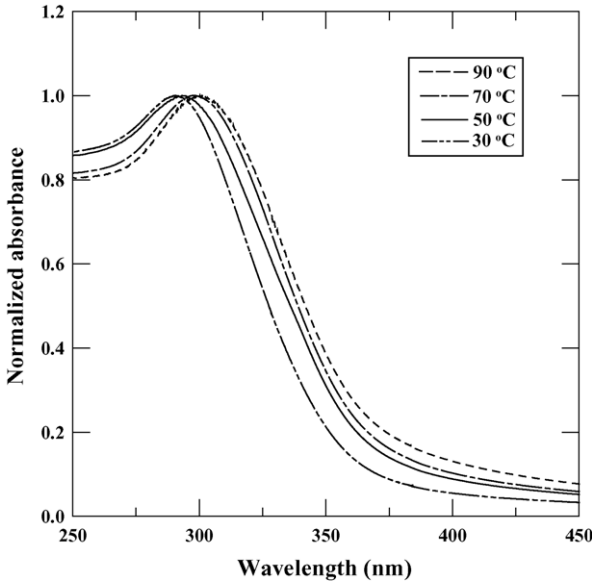

Fig. 8. The UV–vis absorption spectra of CeO_2 particles prepared at different temperatures. $[Ce^{3+}]_0 = 0.2$ M, $[NH_4OH] = 3.0$ M.

This equation indicates that the oxidation of Ce(III) to Ce(IV) is strongly influenced by the oxygen content of atmosphere. Fig. 6 shows the effect of oxygen content on the particle morphology. At 5% O_2 ambient, the resulting particles are all hexagonal. When the oxygen content increases to 50%, few needles appear mixed with hexagonal particles. With increasing the oxygen content, the amount of needle-like particles is increased. Yamashita et al. [2] reported that the needle-like structure was preferred to appear in alkaline media with the presence of hydrogen peroxide via topotactic mechanism [2]. Zhou et al. [26] proposed that the dissolved oxygen most likely caused the slow oxidation of Ce(III) to Ce(IV) and thus resulted in a finer and less agglomerated particles. In other words, at oxygen-rich ambient or by reacting with strong oxidant H_2O_2, it would benefit the formation of needle-like and finer particles. Eventually, as listed in Table 1, the average particle sizes, d_{TEM} and d_{XRD}, consistently decrease with increasing the oxygen content. However, the true mechanism for morphological evolution has not been fully understood.

3.4. Effects of reaction temperature and atmosphere on the lattice relaxation

The lattice relaxation accompanied with reducing the particle size is of great importance and would strongly affect the properties of CeO_2 nanoparticles [31]. Fig. 7 illustrates the dependence of lattice parameter on the crystallite size varying with reaction temperature and atmosphere. As can be found, the lattice parameter decreases consistently with increasing the crystallite size, and is larger than 5.41 Å for bulk CeO_2 crystal [32,33], regardless of changing temperature or atmosphere. Although the oxygen content of atmosphere is indeed an important factor on determining the size and shape of resulting particles, the variation of lattice parameter by oxygen content (within 0.12%) seems, however, less significant than the variation of temperature effect (within 0.27%).

3.5. UV absorption and bandgap energy

As previously reported [34], the size-induced lattice relaxation was usually resulted from the higher percentage of Ce(III) in CeO_2 crystals, which would demonstrate a blue shift of edge absorption in UV–vis absorption spectra. Fig. 8 shows the absorption edge obviously shifts toward shorter wavelength, i.e., blue shift, due to the decrease of particle size by lowering the reaction temperature. The direct bandgap energy can be determined by extrapolating the absorption coefficient (α) to zero [1,17] with

$$(\alpha E_{photon})^2 = C_{dir}(E_{photon} - E_{dir}) \quad (3)$$

where C_{dir} is the absorption constant and E_{dir} is the bandgap energy for direct transition. Conventionally, the absorption coefficient (α) is defined as [1,17]

$$\alpha = \frac{2.303 \mathrm{Abs}\rho}{Lc} \quad (4)$$

where Abs is the absorbance of the sample, c is the sample loading and the L is the path length ($L = 1$ cm). The density of CeO_2, ρ, is taken as 7.28 g/cm^3 [1]. From the plot of $(\alpha E_{photon})^2$ versus E_{photon} (Fig. 9), it reveals that the bandgap decreases from 3.71 to 3.56 eV as the reaction temperature increases from 30 to 90 °C. Furthermore, the indirect bandgap energy can be also determined from the inset of Fig. 9. Similarly, it is found that the indirect bandgap energy

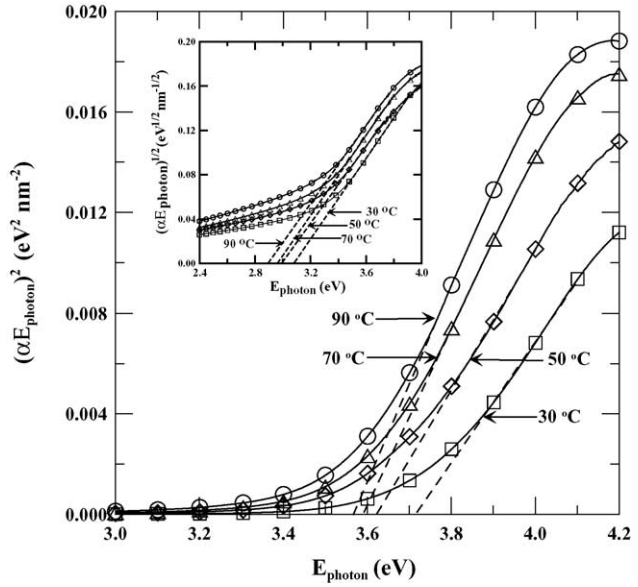

Fig. 9. Plot of $(\alpha E_{photon})^2$ vs. E_{photon} for CeO_2 particles prepared at different temperatures. $[Ce^{3+}]_0$ = 0.2 M, $[NH_4OH]$ = 3.0 M. Inset: Plot of $(\alpha E_{photon})^{1/2}$ vs. E_{photon}.

decreases from 3.08 to 2.89 eV. Comparing the estimated bandgap energies (Fig. 10), it clearly reveals that, due to the quantum size effect, either direct or indirect bandgap energies are mostly larger than values of bulk powders (3.19 eV for direct transition, and 3.01 eV for indirect transition) [1]. In addition, the bandgap energy increases with decreasing the crystallite size by either lowering the reaction temperature or increasing the oxygen content. However, a break is occurred at 21–50% O_2, which encounters the structure and shape transformations for CeO_2 crystals.

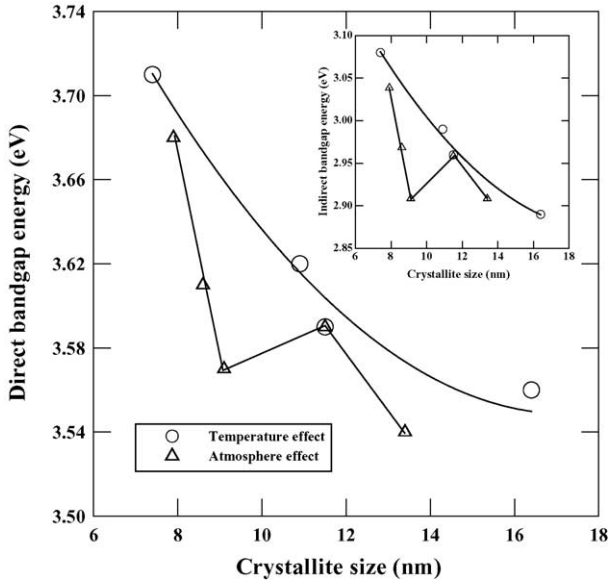

Fig. 10. The dependence of bandgap energies on the crystallite size of CeO_2 particle.

4. Conclusion

From the present results, the properties of prepared CeO_2 nanoparticles are strongly dependent on the reaction temperature and oxygen content of O_2/N_2 atmosphere. Over the whole studied conditions, the resulting particles are characterized to be primary, non-porous and with cubic fluorite structure. The average particle size can be increased by either increasing the reaction temperature or decreasing the oxygen content. Raising the reaction temperature from 30 to 90 °C, the particle shape changes from square-like to hexagonal. Moreover, in oxygen-lean atmosphere, the particles are shaped hexagonal, whereas needles mixed with hexagonal-shaped particles appeared at oxygen content above 50%. The bandgap energies of prepared CeO_2 particles can be approximately modulated by varying the particle size based on the quantum confinement effect, however, the oxygen-induced shape change might cause deviation to some extent.

References

[1] S. Tsunekawa, T. Fukuda, A. Kasuya, Blue shift in ultraviolet absorption spectra of monodisperse CeO_{2-x} nanoparticles, J. Appl. Phys. 87 (3) (2000) 1318–1321.
[2] M. Yamashita, K. Kameyama, S. Yabe, S. Yoshida, Y. Fujishiro, T. Kawai, T. Sato, Synthesis and microstructure of ceria doped ceria as UV filters, J. Mater. Sci. 37 (4) (2002) 683–687.
[3] J. Tashiro, A. Sasaki, S. Akiba, S. Satoh, T. Watanabe, H. Funakubo, M. Yoshimoto, Room-temperature epitaxial growth of indium tin oxide thin films on Si substrates with an epitaxial CeO_2 ultrathin buffer, Thin Solid Films 415 (1/2) (2002) 272–275.
[4] F.H. Garzon, R. Mukundan, E.L. Brosha, Solid-state mixed potential gas sensor: theory, experiments and challenges, Solid State Ionics 136/137 (2000) 633–638.
[5] S. Logothetidis, O. Patsalas, C. Charitidis, Enhanced catalytic activity of nanostructured cerium oxide films, Mater. Sci. Eng. C 23 (6–8) (2003) 803–806.
[6] J. Kašpar, P. Fornasiero, N. Hickey, Automotive catalytic converters: current status and some perspectives, Catal. Today 77 (4) (2003) 419–449.
[7] S.Z. Wang, I. Tatsumi, Improvement of the performance of fuel cells anodes with Sm^{3+} doped CeO_2, Acta Phys.-Chim. Sin. 19 (9) (2003) 844–848.
[8] F. Larachi, J. Pierre, A. Adnot, A. Bernis, Ce 3d XPS study of composite $Ce_xMn_{1-x}O_{2-y}$ wet oxidation catalysts, Appl. Surf. Sci. 195 (1–4) (2002) 236–250.
[9] M.T. Dario, A. Bachiorrini, Interaction of mullite with some polluting oxides in diesel vehicle filters, Ceram. Int. 25 (6) (1999) 511–516.
[10] R. DiMonte, P. Fornasiero, M. Graziani, J. Kašpar, Oxygen storage and catalytic NO removal promoted by CeO_2-containing mixed oxides, J. Alloys Compd. 277 (1998) 877–885.
[11] G.R. Bamwenda, H. Arakawa, Cerium dioxide as a photocatalyst for water decomposition to O_2 in the presence of Ce^{4+}_{aq} and Fe^{3+}_{aq} species, J. Mol. Catal. A 161 (1/2) (2000) 105–113.
[12] N.C. Wu, E.W. Shi, Y.Q. Zheng, W.J. Li, Effect of pH of medium on hydrothermal synthesis of nanocrystalline cerium(IV) oxide powders, J. Am. Ceram. Soc. 85 (10) (2002) 2462–2468.
[13] M. Hirano, E. Kato, Hydrothermal synthesis of nanocrystalline cerium(IV) oxide powders, J. Am. Ceram. Soc. 82 (3) (1999) 768–788.

[14] Y.C. Zhou, M.N. Rahaman, Hydrothermal synthesis and sintering of ultrafine CeO_2 powders, J. Mater. Res. 8 (7) (1993) 1680–1686.
[15] S. Lakhwani, M.N. Rahaman, Hydrothermal coarsening of CeO_2 particles, J. Mater. Res. 14 (4) (1999) 1455–1461.
[16] Y. Hakuta, S. Onai, H. Terayama, T. Adschiri, K. Arai, Production of ultra-fine ceria particles by hydrothermal synthesis under supercritical conditions, J. Mater. Sci. Lett. 17 (14) (1998) 1211–1213.
[17] T. Masui, K. Fujiwara, K.I. Machida, G.Y. Adachi, T. Sakata, H. Mori, Characterization of cerium(IV) oxide ultrafine particles prepared using reversed micelles, Chem. Mater. 9 (10) (1997) 2197–2204.
[18] L. Yin, Y. Wang, G. Pang, Y. Koltypin, A. Gedanken, Sonochemical synthesis of cerium oxide nanoparticles—effect of additives and quantum effect, J. Colloid Interf. Sci. 246 (1) (2002) 78–84.
[19] H. Xu, L. Gao, H. Gu, J. Guo, D. Yan, Synthesis of solid, spherical CeO_2 particles prepared by the spray hydrolysis reaction method, J. Am. Ceram. Soc. 85 (1) (2002) 139–144.
[20] X.D. Zhou, W. Huebner, H.U. Anderson, Room-temperature homogeneous nucleation synthesis and thermal stability of nanometer single crystal CeO_2, Appl. Phys. Lett. 80 (20) (2002) 3814–3816.
[21] E. Matijević, W.P. Hsu, Preparation and properties of monodispersed colloidal particles of lanthanide compounds, J. Colloid Interf. Sci. 118 (2) (1987) 506–523.
[22] P.L. Chen, I.W. Chen, Reactive cerium(IV) oxide powders by the homogeneous precipitation method, J. Am. Ceram. Soc. 76 (6) (1993) 1577–1583.
[23] J.G. Li, T. Ikegami, Y.Y. Wang, T. Mori, Reactive ceria nanopowders via carbonate precipitation, J. Am. Ceram. Soc. 85 (9) (2002) 2376–2378.
[24] N. Uekawa, M. Ueta, Y.J. Wu, K. Kakegawa, Synthesis of CeO_2 spherical fin particles by homogeneous precipitation method with polyethylene glycol, Chem. Lett. (8) (2002) 854–855.
[25] H.I. Chen, H.Y. Chang, Homogeneous precipitation of cerium dioxide nanoparticles in alcohal–water mixed solvents, Colloid Surf A 242 (1–3) (2004) 61–69.
[26] X.D. Zhou, W. Huebner, H.U. Anderson, Processing of nanometer-CeO_2 particles, Chem. Mater. 15 (2) (2003) 378–382.
[27] B. Djuričić, S. Pickering, Nanostructured cerium oxide: preparation and properties of weakly agglomerated powders, J. Eur. Ceram. Soc. 19 (11) (1999) 1925–1934.
[28] Z.L. Wang, X. Feng, Polyhedral shapes of CeO_2 nanoparticles, J. Phys. Chem. B 107 (49) (2003) 13563–13566.
[29] Z.L. Wang, Transmission electron microscopy of shape-controlled nanocrystals and their assemblies, J. Phys. Chem. B 104 (6) (2003) 1153–1175.
[30] N.B. Kirk, J.V. Wood, The effect if the calcination process on the crystallite shape of sol–gel cerium oxide used for glass polishing, J. Mater. Sci. 30 (1995) 2171–2175.
[31] V. Perebeinos, S.W. Chan, F. Zhang, 'Madelung model' prediction for dependence of lattice parameter on nanocrystal size, Solid State Commun. 123 (6/7) (2002) 295–297.
[32] X.D. Zhou, W. Huebner, Size-induced lattice relaxation in CeO_2 nanoparticles, Appl. Phys. Lett. 79 (21) (2001) 3512–3514.
[33] S. Tsunekawa, R. Sahara, Y. Kawazoe, K. Ishikawa, Lattice relaxation of monosize CeO_{2-x} nanocrystalline particles, Appl. Surf. Sci. 152 (1/2) (1999) 53–56.
[34] S. Tsunekawa, R. Sivamohan, T. Ohsuna, A. Kasuya, H. Takahashi, K. Tohji, Ultraviolet absorption spectra of CeO_2 nano-particles, Mater. Sci. Forum 315–317 (1999) 439–445.